Contents lists available at SciOpen

Food Science and Human Wellness

journal homepage: https://www.sciopen.com/journal/2097-0765

China Food Publishing Co.

Syringa pubescens Turcz. ethyl acetate extract improves non-alcoholic steatohepatitis by regulating the Nrf2, IκBα and TGF-β1 signaling pathways

Weidong Xu[a], Yanfang Wu[b,*], Jiansheng Xiong[a], Jiameng Zhang[a], Zichen Zhang[a], Xinyi Guan[a], Suya Zhang[a], Xinsheng Wang[a,*], Pu Liu[a], Enguo Fan[c,*]

[a] College of Chemistry and Chemical Engineering, Henan University of Science and Technology, Luoyang 471000 China
[b] College of Basic Medical and Forensic Medicine, Henan University of Science and Technology, Luoyang 471000 China
[c] Department of Microbiology and Parasitology, Institute of Basic Medical Sciences, Chinese Academy of Medical Sciences/School of Basic Medicine, Peking Union Medical College, Beijing 100005 China

ARTICLE INFO

Article history:
Received 27 January 2024
Received in revised form 21 February 2024
Accepted 7 April 2024

Keywords:
Syringa pubescens Turcz
Nonalcoholic steatohepatitis,
Nuclear erythroid 2-related factor 2
Nuclear factor kappa B
Transforming growth factor β1

ABSTRACT

The flower of *Syringa pubescens* Turcz. (SP), was used as both medicine and food in China, exhibited various biological activities. However, it remains unknown whether SP affects ameliorative nonalcoholic steatohepatitis (NASH). In this study, the improvement of SP ethyl acetate extract (SPE) on NASH was evaluated and the potential mechanisms were explored. The glycosides of SPE were determined by HPLC method. HepG2 cell lines were treated with free fatty acid to clarify the improvement effect and mechanisms of SPE on NASH *in vitro*. C57BL/6J mice were treated by 60% kcal high-fat diet (HFD) combined with carbon tetrachloride (CCl_4) to establish the NASH model *in vivo*. The results showed SPE could inhibit the hepatic injury and lipid steatosis by decreasing the levels of alanine aminotransferase, aspartate aminotransferase, triglyceride and total cholesterol in *vitro* and *in vivo*. The SPE suppressed the oxidative stress and inflammation by restraining the generation of reactive oxygen species, malondialdehyde, interleukin (IL)-1β, IL-6 and tumor necrosis factor-α (TNF-α) and enhancing the activity of antioxidant enzymes including superoxide dismutase, catalase and glutathione peroxidase in NASH model. Moreover, SPE declined the level of fibrosis markers including hydroxyproline, type I collagen and α-smooth muscle actin (α-SMA) in HFD combined CCl_4-induced mice. Mechanically, SPE inhibited hepatocellular Kelch like ECH associated protein 1 expression and promoted nuclear erythroid 2-related factor 2 (Nrf2) nuclear translocation, which suppressed the phosphorylation of IκBα/NF-κB. In addition, SPE down-regulated the level of transforming growth factor β1 (TGF-β1) and phosphorylation of Smad2 to mitigate fibrosis. In brief, SPE could significantly alleviate lipid accumulation, oxidative stress, inflammation and fibrosis *via* regulating Nrf2/HO-1, IκBα/NF-κB and TGF-β1/Smad2 pathways in the progression of NASH, which indicated that SPE had the potential to be a novel and effective drug or food supplements for the improvement of NASH.

1. Introduction

Nonalcoholic steatohepatitis (NASH), a chronic liver disease, is a critical stage in nonalcoholic fatty liver disease (NAFLD), commonly accompanied with different severity of steatosis, inflammation, and fibrosis[1-2]. The prevalence of NASH has been increasing in the past 2 decades and replaced viral hepatitis as the leading cause of increased incidence and mortality of cirrhosis and hepatocellular carcinoma[3]. NASH is also a serious risk factor for many metabolic diseases, such as obesity, cardiovascular disease, and type 2 diabetes mellitus (T2DM)[4].

The etiology and pathogenesis of NASH are complicated. Multiple factors such as lipid accumulation, oxidative stress,

* Corresponding authors.
E-mail address: wyf245@163.com (Y.F. Wu); wxs501@gmail.com (X.S. Wang); enguo.fan@ibms.pumc.edu.cn (E.G. Fan)
Peer review under responsibility of Beijing Academy of Food Sciences.

SciOpen Publishing services by Tsinghua University Press

http://doi.org/10.26599/FSHW.2024.9250244

inflammation, and matrix deposition jointly lead to the development of NAFLD to NASH. Previous studies have shown that oxidative stress plays a key role in NASH. Persistent oxidative stress leads to inflammation and fibrosis[5-6]. Nuclear erythroid 2-related factor 2 (Nrf2) pathway was found to play a dual role in antioxidant defense and liver lipid metabolism regulation in NASH[7]. During oxidative stress or other chemical stimulation, Nrf2 translocates into the nucleus, where it binds to the related gene promoter antioxidant response element (ARE) sequence. It then induces the expression of downstream genes involved in antioxidants and detoxification enzymes such as superoxide dismutase (SOD), catalase (CAT), glutathione peroxidase (GSH-Px), heme oxygenase 1 (HO-1) and NAD(P)H-quinone oxidoreductase 1 (NQO1)[8]. Accumulating evidences suggest that Nrf2 impedes the activity of nuclear factor kappa B (NF-κB), a crucial transcription factor in inflammation[9-10]. Under normal conditions, NF-κB forms a complex with inhibitory subunit of NF-κB family proteins (IκBs) in the cytoplasm to maintain low activity. When cells are stimulated, NF-κB can be phosphorylated by activation of IκB kinase. Phosphorylated NF-κB is released as dimers (p65 and p50) and translocated from the cytoplasm to the nucleus, followed by transcription of target genes such as pro-inflammatory cytokines (interleukin-1β (*IL-1β*), interleukin-6 (*IL-6*) and tumor necrosis factor-α (*TNF-α*)) and inflammation-related enzymes inducible nitric oxide synthase (*iNOS*) and cyclooxygenase-2 (*COX-2*)[11]. Furthermore, liver fibrosis is related to NF-κB pathway. Hepatic macrophages are activated by inflammation[6]. Macrophage-derived transforming growth factor β1 (TGF-β1) is the most potent known fibrogenic agonist. Smads are crucial family proteins in mediating intracellular TGF-β1 signaling. TGF-β1 induces phosphorylation of Smad2 and Smad3. Then cytoplasmic Smad4 forms a complex with phosphorylated Smad2 and Smad3[12]. The translocation of the complex to the nucleus regulates the expression of profibrotic proteins such as α-smooth muscle actin (α-SMA) and type I collagen (Col-I), resulting in the increased extracellular matrix deposition and ultimately liver fibrosis in NASH[13].

Despite the increasing incidence of NASH, there are no specific therapies for the NASH[14]. In the past few years, researchers have proposed several molecular drugs with different targets for NASH pathogenesis, including glucagon-like peptide-1 receptor analogues liraglutide[15], acetyl-CoA carboxylase inhibitors GS-0976[16] and adiponectin receptors agonist[17]. However, these candidates have shown severe side effects or limited drug efficacy in the treatment of NASH. Interestingly, people in Asia have a habit of eating healthcare foods to prevent liver disease. Many natural functional plant foods have the effect of preventing hyperlipidemia and protecting the liver[18].

Syringa pubescens Turcz. (SP) is widely distributed in the mountains of China. The dried flower of SP is often used as flower tea and pastry supplies for healthcare in Henan, China[19]. To date, modern scientific studies have shown that SP has a variety of biological and pharmacological properties, including antioxidant properties, hepatoprotective, anti-inflammatory and antibacterial activities[20-22]. Moreover, the tea bag and healthcare candy prepared using SP flower have been proved possessing hepatoprotective and antihypertensive functions, which was patented by our research group (CN201310060752.2, CN201410515099.9). Therefore, SP may equip with the potential in the improvement of NASH.

In this work, we established both *in vitro* and *in vivo* NASH models to explore the therapeutic effects and underlying mechanisms of SP ethyl acetate extract (SPE) on NASH. The findings obtained from this study offer new insight into the anti-NASH application of SPE and manifest the potential of SPE in the treatment of NASH.

2. Materials and methods

2.1 Chemicals and reagents

The 3-(4,5-dimethylthiazol-2-yl)-2,5-diphenyltetrazolium bromide (MTT) and PVDF membranes (Immobilon-P, 0.45 μm) were purchased from Sigma-Aldrich (Saint Louis, MO, USA). Authentic standards of salidroside, syringoside, echinacoisde, forsythoside B, verbascoside, isoacteoside, and oleuropein were obtained from Chengdu Biopurify Phytochemicals Ltd. (Chengdu, China). Ultra-sensitive ECL chemiluminescent substrate, 4′,6-diamidino-2-phenylindole (DAPI) were from Solarbio (Beijing, China). Primary antibodies against Kelch like ECH associated protein 1 (Keap1, ab227828), Nrf2 (ab62352), HO-1 (ab52947) and NQO1 (ab80588), p-Smad2 (ab280888), Smad2 (ab119907) and *β*-actin (ab8227) were from Abcam (Cambridge, MA, USA), TGF-β1 (AF1027) and PCNA (AF0239) were from Affinity (Cincinnati, OH, USA), α-smooth muscle actin (α-SMA, sc-53142) were from Santa Cruz (Dallas, Texas, USA). The horseradish peroxidase (HRP)-conjugated secondary antibodies (SA00001-1, SA00001-2) were from Proteintech (Wuhan, China). Dulbecco's modified Eagle's medium (DMEM) and fetal bovine serum (FBS) were obtained from Hyclone (Waltham, MA, USA), penicillin-streptomycin solution and trypsin (0.25% EDTA) were purchased from Coolaber (Beijing, China). High-fat diet (HFD, No. D12492) consisting of 60% kcal fat was purchased from Research Diets, Inc. (Middlesex County, NJ, USA). The major compositions in the HFD were lard (31.66%, *m*/*m*), casein (25.84%, *m*/*m*) and maltodextrin 10 (16.15%, *m*/*m*). The regular diet (No. 1010002) was purchased from Xietong Pharmaceutical Bio-engineering Co., Ltd. (Nanjing, China).

2.2 Plant extraction preparation

Syringa pubescens Turcz. (Luoyang, China) was authenticated by Prof. Yanfang Wu and stored in the College of Basic Medicine and Forensic Medicine, Henan University of Science and Technology. The samples were shade dried at room temperature and pulverized, then passed through a 60-mesh. The samples were refluxed with 70% ethanol (*V*/*V*) for 1 h (3 times). After filtration, the filtrate was concentrated until it was alcohol-free, and then the liquid was sequentially extracted with petroleum ether, ethyl acetate, and water saturation of *n*-butyl alcohol. The petroleum ether, ethyl acetate and *n*-butyl alcohol fractions were concentrated and evaporated to dried powder separately to obtain SP petroleum ether extract (SPP), SPE and SP *n*-butyl alcohol extract (SPB). The samples were stored at 4 °C before use.

2.3 Phytochemical analysis

High performance liquid chromatography (HPLC) method was conducted according to our previous study with a slight adjustment[23]. In brief, SPP, SPE and SPB were ultrasonically dissolved in methanol to obtain sample solutions (5 mg/mL). A mixed

standard solution containing salidroside, syringoside, echinacoside, forsythoside B, verbascoside, isoacteoside, and oleuropein was prepared. The sample and standard solutions were diluted and filtered through a 0.22 μm membrane before analysis. HPLC analysis was performed on an Eclassical 3 200 HPLC system (Dalian Elite Analytical Instrument Co., Ltd., Dalian, China) equipped with an ultraviolet detector, an autosampler, a binary pump, and a column oven. The separation of active compounds was conducted with an Elite Supersil ODS2 column (4.6 mm × 250 mm, 5 μm, Dalian Elite Analytical Instrument Co., Ltd., Dalian, China). Acetonitrile and acetic acid water (0.5%, *V*/*V*) were used as mobile phases A and B, respectively. The gradient program was established as follows: 0–5 min, 8%–17% A; 5–18 min, 17%–21% A; 18–35 min, 21%–24% A; 35–45 min, 24% A. Finally, the starting conditions were kept for 5 min as a re-equilibration step. The detection wavelength was developed as follows: 0–10 min, 276 nm; 10–29 min, 332 nm, 29–45 min, 285 nm. The flow rate was set at 1.0 mL/min, the injection volume was 5 μL and the column temperature was kept at 30 ℃.

2.4 Cell line and culture

HepG2 cell line was obtained from ATCC with short tandem repeat (STR) identification report. Cells were cultured in DMEM supplemented with 10% FBS and 1% penicillin-streptomycin under a humidified incubator with 5% CO_2 at 37 ℃.

2.5 Cell viability assay

The extracts (SPP, SPE and SPB) were dissolved in the DMEM medium containing 10% fetal bovine serum with the concentrations of 37.5, 75.0 and 150.0 μg/mL, respectively. Cells were cultured in 96-well plates for 24 h, and then treated with or without 1 mmol/L free fatty acid (FFA) mixture (palmitate:oleate = 1:2) and extract medium for 24 h (treated with FFA, FFA group; treated without FFA, control group). Then the cell viability was evaluated by MTT assay[24]. The 10 μL MTT (5 mg/mL) was added to each well, after 4 h incubation at 37 ℃, the medium was removed, and 100 μL DMSO was added to dissolve the precipitate. The absorbance was measured at 570 nm by Microplate Reader (Epoch, BioTek, Winooski, VT, USA).

2.6 Animals and treatment

Six weeks old (16–18 g) male C57BL/6J mice were purchased from Henan SCBS Biotechnology ([SPF, SCXK (YU)-2020-0005], Henan, China). All animals were arranged in SPF environment at (24 ± 1) ℃ (relative humidity: 40%–70%), with a 12 h light and 12 h dark cycle. All mouse studies conformed to the Animal Ethics Committee, Henan University of Science and Technology (Approval No. 20230320). The NASH mouse models were induced by feeding mice with a HFD (60% kcal from fat) for 12 weeks[25]. After 1 week of acclimatization, mice were randomly divided into 6 group: control group (fed with a regular diet, CON), model group (fed with HFD, MOD), positive control group (fed with HFD + silymarin at 60 mg/kg·day, SILY), low-dose group (250 mg/kg SPE, oral gavage daily, SPEL), middle-dose group (500 mg/kg SPE, oral gavage daily, SPEM) and high-dose group (1 000 mg/kg SPE, oral gavage daily, SPEH)[26]. Throughout the experimental period, mice in the 5 groups except for CON group were fed with HFD. Simultaneously, the mice in the CON group were intraperitoneally injected with olive oil, and the other mice were intraperitoneally injected with CCl_4 (0.2 μL/g, dissolved in olive oil) once a week for 12 weeks. For the last 4 weeks, mice were orally administered with SPE (dissolved in 0.5% CMC-Na solution) or silymarin once a day. Body weight was recorded at every 4 days intervals until the end of the experiment. Mice were sacrificed at the end of the experiment, and plasma and tissue were collected.

2.7 Oil red O (ORO) staining of HepG2 cell

HepG2 cells were washed with cold phosphate-buffered saline (PBS) and fixed in 4% paraformaldehyde for 20 min at room temperature. After washing, cells were rinsed with 60% isopropanol for 5 min and then dyed in 0.5% ORO solution for 20 min and each group was photographed.

2.8 Measurement of intracellular ROS

The level of ROS was detected using fluorescent probe 2′,7′-dichloro-dihydro-fluorescein diacetate (DCFH-DA, Nanjing Jian Cheng Bioengineering Institute, Nanjing, China). Cells were collected and incubated with DCFH-DA for 30 min at 37 °C in the dark. Intracellular ROS fluorescence intensity was observed and photographed by an inverted fluorescence microscope (IX73, Olympus, Japan).

2.9 Biochemical analysis

Serum, liver tissues and cells lysates were individually collected. The levels of alanine aminotransferase (ALT), aspartate aminotransferase (AST), triglyceride (TG), total cholesterol (TC), high-density lipoprotein cholesterol (HDL-C), low-density lipoprotein cholesterol (LDL-C), malondialdehyde (MDA), superoxide dismutase (SOD), catalase (CAT), glutathione peroxidase (GSH-Px) and total antioxidizing capability (T-AOC) were tested with commercial kits according to the manufacturer's instructions (Nanjing Jian Cheng Bioengineering Institute, Nanjing, China). Each treatment was replicated 6 times.

The levels of IL-1β, IL-6 and TNF-α in cells, mice serum and liver tissues were detected using commercial reagent kits (Nanjing Jian Cheng Bioengineering Institute, Nanjing, China). Each treatment was repeated 6 times.

2.10 Histological analysis

For hematoxylin and eosin (H&E), ORO, Sirius red and Masson staining, frozen liver tissues were embedded in paraffin. Embedded tissues were sectioned into 5 μm-thick slices and attached on glass slides. Then the sections were stained with H&E, ORO, Sirius red and Masson for microscopic assessment, respectively. The H&E staining results were used to evaluate the NAFLD activity score (NAS) system[27].

2.11 Immunofluorescent staining assay

HepG2 cells were fixed in 4% formaldehyde for 15 min and then permeabilized with 0.5% Triton X-100 for 30 min at room temperature. After washing with PBS, cells were incubated with

primary antibodies overnight at 4 ℃. A fluorescein secondary antibody conjugated to primary antibodies was then added for 2 h in the dark, and the cells were counterstained with DAPI for 10 min. Then the fluorescent expression was observed under a laser confocal microscopy (Fluoview FV1 200, Olympus, Japan).

2.12 Cytoplasm and nucleus proteins fractionation

The fractionation of cytoplasm and nucleus proteins was conducted according to the manufacturer's instructions (Solarbio, Beijing, China).

2.13 Western blot analysis

Liver tissues and HepG2 cells were lysed with RIPA buffer to extract the total tissue and cellular proteins. The protein content was quantified by the bicinchoninic acid (BCA) protein assay kit (Solarbio, Beijing, China). Then, proteins were separated by sodium dodecyl sulfate polyacrylamide gel electrophoresis (SDS-PAGE) and transferred onto PVDF membranes. After that, membranes were blocked with 5% milk, and subsequently incubated with primary antibodies diluted in PBST. Thereafter, the protein blots were incubated with HRP-conjugated secondary antibody at room temperature for 1 h. Finally, the bands of proteins were detected by ultra-sensitive ECL chemiluminescent substrate and imaged with the Tanon 4600 System (Tanon, Shanghai, China). The grey scales of the bands were analyzed using ImageJ software. The grey value of protein bands was normalized to internal control protein bands to obtain the average ratios, and the ratios were further normalized to the control group to show the quantitative analysis results.

2.14 Molecular docking

Molecular docking analysis was performed to investigate the possible binding mode between the 7 SPE bioactive glycosides and the 5 protein structures (Keap1, NF-κB, TGFβ1, Smad2, α-SMA). The crystal structure of Keap1 (code 4L7B), NF-κB (code 1NFI), TGF-β1 (code 3TZM), Smad2 (code 5XOD) and α-SMA (code 4PKG) were obtained from the PDB website (http://www.rcsb.org/). 3D structure SDF files of each ligand were obtained from the PubChem database (https://www.ncbi.nlm.nih.gov/pccompound). ChemBio3D 16.0 software was used for conformational optimization and the structure files were saved in PDB format. AutoDock Vina. software was used for molecular docking research. The size and center of the grid have been determined according to the position of amino acid residues that interact with the ligand. PyMOL 2.2.0 software was used for visual analysis of docking results[28-29].

2.15 Statistical analysis

Results were expressed as mean ± standard deviation (SD) and analyzed using GraphPad 8.0.1 software. Student's *t*-tests were used to compare the means of 2 groups; multigroup mean samples were compared using One-Way analysis of variance (ANOVA). *P*-value < 0.05 was considered as significant.

3. Results

3.1 Phytochemical analysis

The 7 bioactive glycosides of SPP, SPE and SPB were detected by HPLC. The representative HPLC chromatograms of SPP, SPE, SPB and 7 standard substances were showed in Figs. 1A-D. As shown in Table S1, the highest content of glycosides was found in SPE. The contents of salidroside, syringoside, echinacoside, forsythoside B, verbascoside, isoacteoside, and oleuropein in SPE were (13.371 ± 0.185), (0.250 ± 0.024), (7.460 ± 0.075), (8.201 ± 0.081), (1.437 ± 0.083), (0.564 ± 0.031) and (10.629 ± 0.121) mg/g, respectively. Notably, the syringoside was identified for the first time in SP.

3.2 SPE improved hepatocyte damage and lipid accumulation in FFA-induced HepG2 cells

To evaluate the improvement effect of SPP, SPE and SPB on hepatocyte. HepG2 cells were treated with the 3 SP extracts for 24 h with or without FFA. As shown in Fig. 2A, the cell viability of groups treated with 3 SP extracts increased. Moreover, cells treated with 150 μg/mL of SPP, SPE and SPB restored cell viability up to 64.0%, 104.3% and 81.3%. Our previous work showed that SPE had better anti-inflammatory and antioxidant effects than SPP and SPB[30]. Thus, SPE was selected for subsequent experiments.

As shown in Figs. 2B and C, the levels of TG and TC were highest in FFA-only group ((0.124 ± 0.014), (0.246 ± 0.011) mmol/g prot), while the indexes were decreased with SPE administration in a dose dependent manner. ORO staining results exhibited severely lipid accumulation in FFA-cultured cells (Figs. 2D and E). However, after the treatment with SPE, the number of lipid droplets significantly decreased. Meanwhile, the level of cellular AST and ALT were dramatically increased after FFA induction. And the results showed that SPE dose-dependently reduced AST and ALT levels compared with FFA group (Figs. 2F and G).

3.3 SPE suppressed oxidative stress and inflammation in FFA-induced HepG2 cells

To investigate the effect of SPE on antioxidant and anti-inflammatory activities, the oxidative stress markers and pro-inflammatory cytokines in cells from all groups were measured and the results were shown in Fig. 3. ROS played a significant mediator for oxidative stress and inflammatory, which was measured and shown in Figs. 3A and B. The fluorescence intensity of ROS was found to be significantly reduced in FFA-treated hepatocytes in the presence of SPE ($P < 0.001$). Similarly, the level of MDA increased from (54.139 ± 3.075) to (108.369 ± 2.766) mmol/g prot (Fig. 3C). The SPE treatment groups decreased the levels of ROS and MDA in a dose dependent manner. Correspondingly, FFA decreased the levels of SOD, CAT and GSH-Px, which were increased after SPE treatment. (Figs. 3D-F). In particular, the CAT level in SPEH group was higher than that of the control group. Moreover, the results revealed all the pro-inflammatory cytokines IL-1β, IL-6 and TNF-α in FFA group

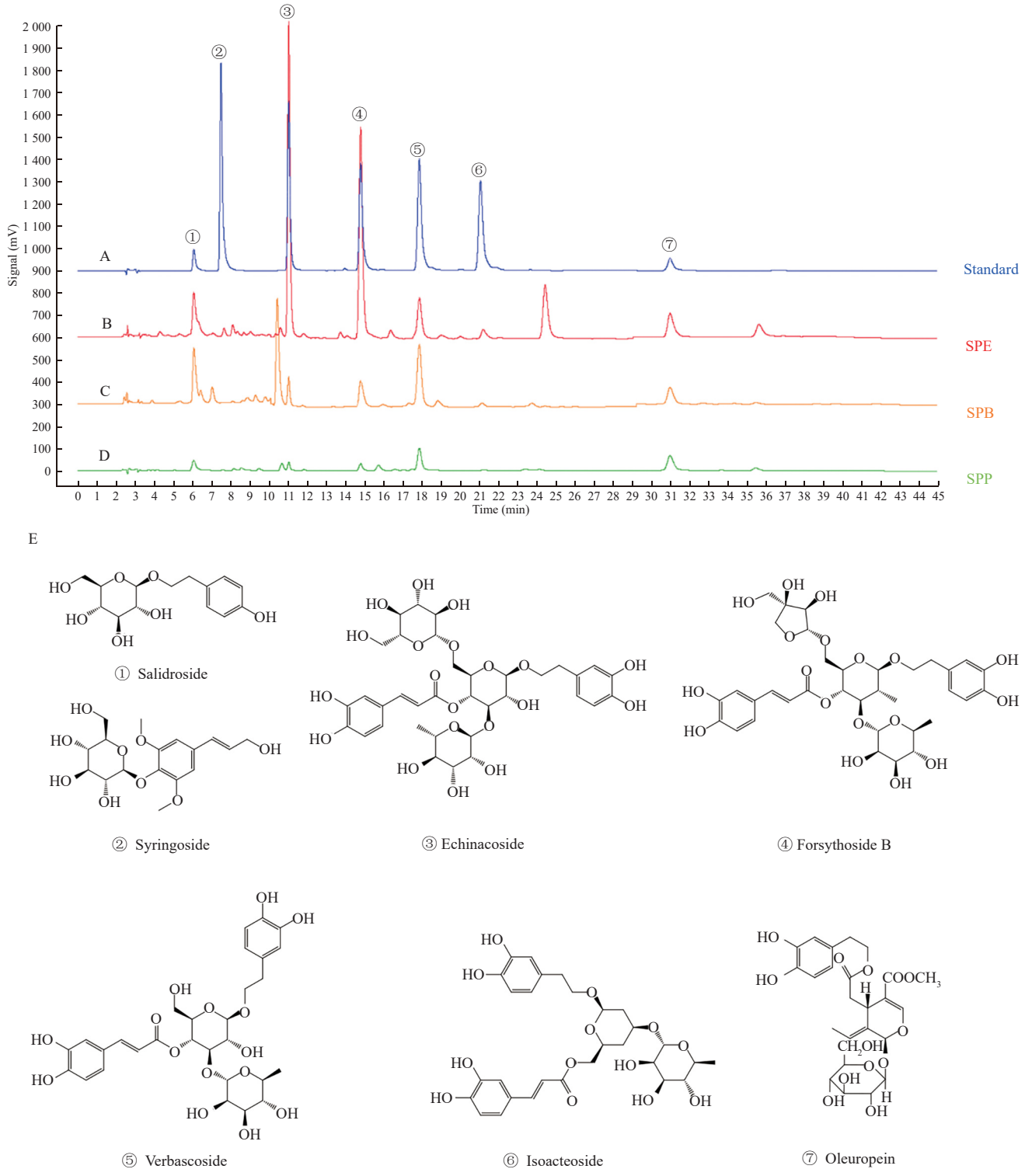

Fig. 1 The representative HPLC chromatogram of SPE, SPB, SPP and 7 standard substances. HPLC chromatogram of (A) standard substances, (B) SPE, (C) SPB, (D) SPP. (E) chemical structures of the 7 standard substances.

((14.197 ± 0.797), (18.832 ± 0.602), (18.711 ± 0.981) pg/mL) were significantly higher than those of the control group ((4.569 ± 0.361), (7.096 ± 0.293), (9.297 ± 0.424) pg/mL). SPE administration decreased the over-production of the pro-inflammatory cytokines (Figs. 3G-I). The results indicated SPE effectively inhibited oxidative stress and inflammation in FFA-induced HepG2 cells.

3.4 SPE regulated Nrf2 and NF-κB pathways in FFA-induced HepG2 cells

Previous studies demonstrated Nrf2 played a critical effect on antioxidative stress and inhibited the phosphorylation of NF-κB, which was a pivotal marker in the development of inflammation[9].

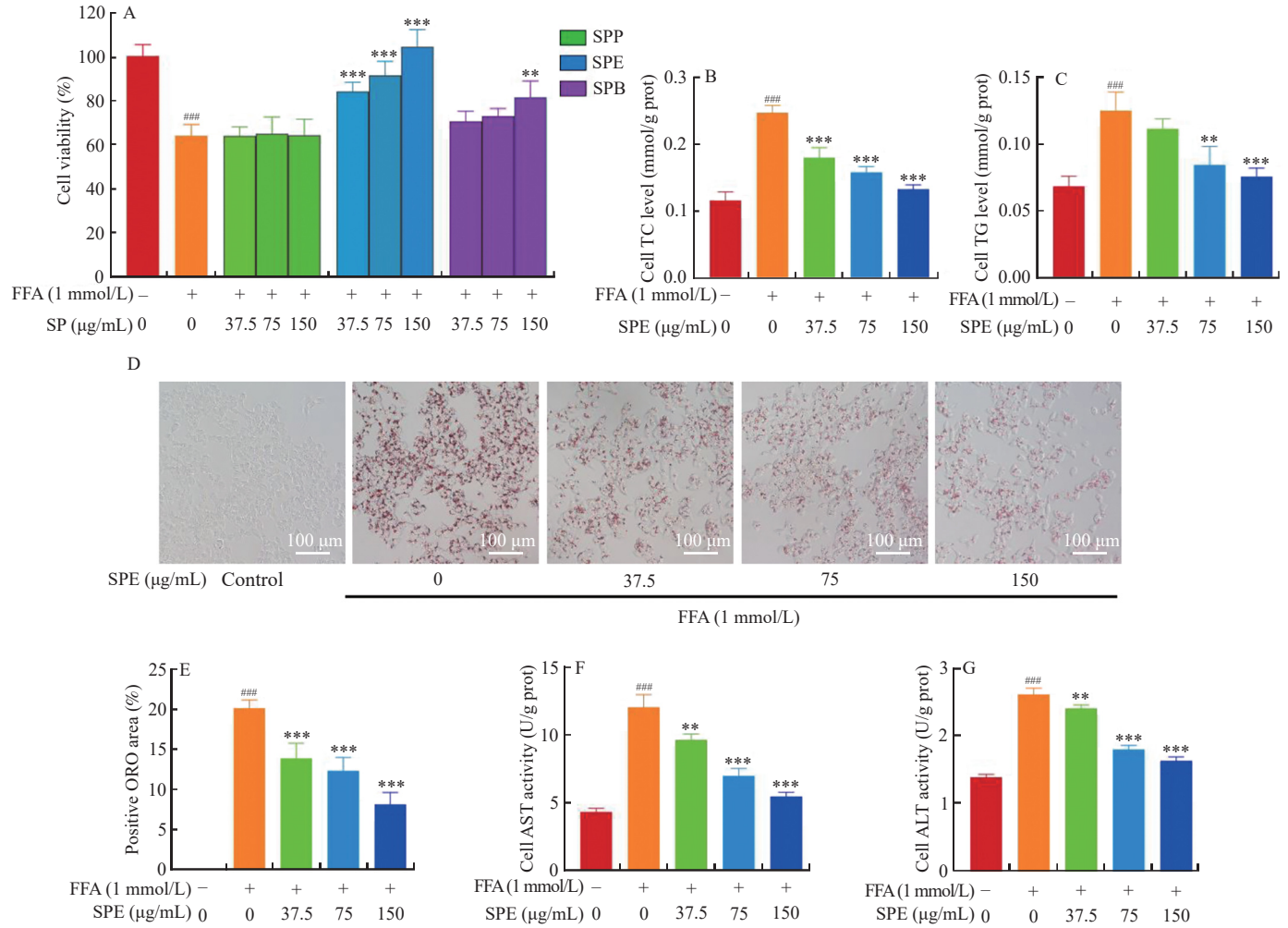

Fig. 2 SPE inhibited lipid accumulation in FFA-induced HepG2 cells. (A) Cells viability. (B) Cells TC level. (C) Cells TG level. (D) Cells ORO staining (200×). (E) Quantitative analysis of cells ORO staining. (F) Cells AST activity. (G) Cells ALT activity. Data were presented as the mean ± SEM ($n = 6$). $^{###}P < 0.001$ *vs*. control group; $^{**}P < 0.01$, and $^{***}P < 0.001$ *vs*. FFA group.

To elucidate the underlying mechanisms in the beneficial effect of SPE in HepG2 cells, the Nrf2 and NF-κB pathway relative proteins were investigated. Compared with the FFA group, SPE treatment suppressed the expression of Keap1 and enhanced the nuclear-Nrf2 (Nu-Nrf2) expression, which suggested SPE promoted the nuclear translocation of Nrf2 (Figs. 4A-F). Correspondingly, SPE upregulated the downstream target proteins HO-1 and NQO1 expressions. The results of immunofluorescence further confirmed that SPE assisted Nrf2 transferring into the nucleus in turn to control the downstream protein expression (Fig. 4G). In addition, SPE significantly inhibited the levels of p-IκBα and p-p65 in a dose-dependent manner compared with the FFA-treated HepG2 cells (Figs. 4H-L). Those results confirmed that SPE could improve HepG2 cells from NASH *via* activating Nrf2 and suppressing NF-κB pathways *in vitro*.

3.5 SPE decreased body and organs weight in HFD combined CCl_4 (HC)-induced mice

HC-induced mice were used to evaluate the amelioration of SPE on NASH *in vivo*. As shown in Fig. S1A, HC could obviously induce obesity, while SPE treatment reversed the increase in body weight in a dose-dependent manner. Eventually, at the 12th week, the body weight of the mice in MOD group reached (33.84 ± 1.92) g, while those of the SPEL, SPEM, SEPH and SILY groups were (31.00 ± 2.29), (29.61 ± 1.28), (28.16 ± 2.08) and (28.64 ± 2.35) g, respectively. The differences of body were visual in Fig. S1B, mice in the MOD group had a longer and wider body size than the other 5 groups. The mice from the CON and SPEH group were in similar size. The changes were also exhibited in liver tissues. The liver of CON group mice was red and its surface was smooth and soft, while the liver in MOD group mice was yellow and its surface was rough and hard. And SPE or silymarin significantly reduced liver volume and softened liver texture (Fig. S1C). The weight of liver, heart and abdominal fat in the MOD group was significantly higher than those of the CON group mice. Besides, SPE reduced the organs (liver and heart) and adipose tissue weight (Table S2, $P < 0.001$). In addition, the liver/body ratio was highest in MOD group mice showed a higher of weight, which was significantly reduced by SPE treatment (Table S2, $P < 0.01$).

3.6 SPE ameliorated liver injury and steatosis in HC-induced mice

To evaluate the improvement of SPE on liver injury and steatosis *in vivo*, liver sections were stained with H&E and ORO. As shown in Fig. 5A, the liver sections stained with H&E demonstrated that after

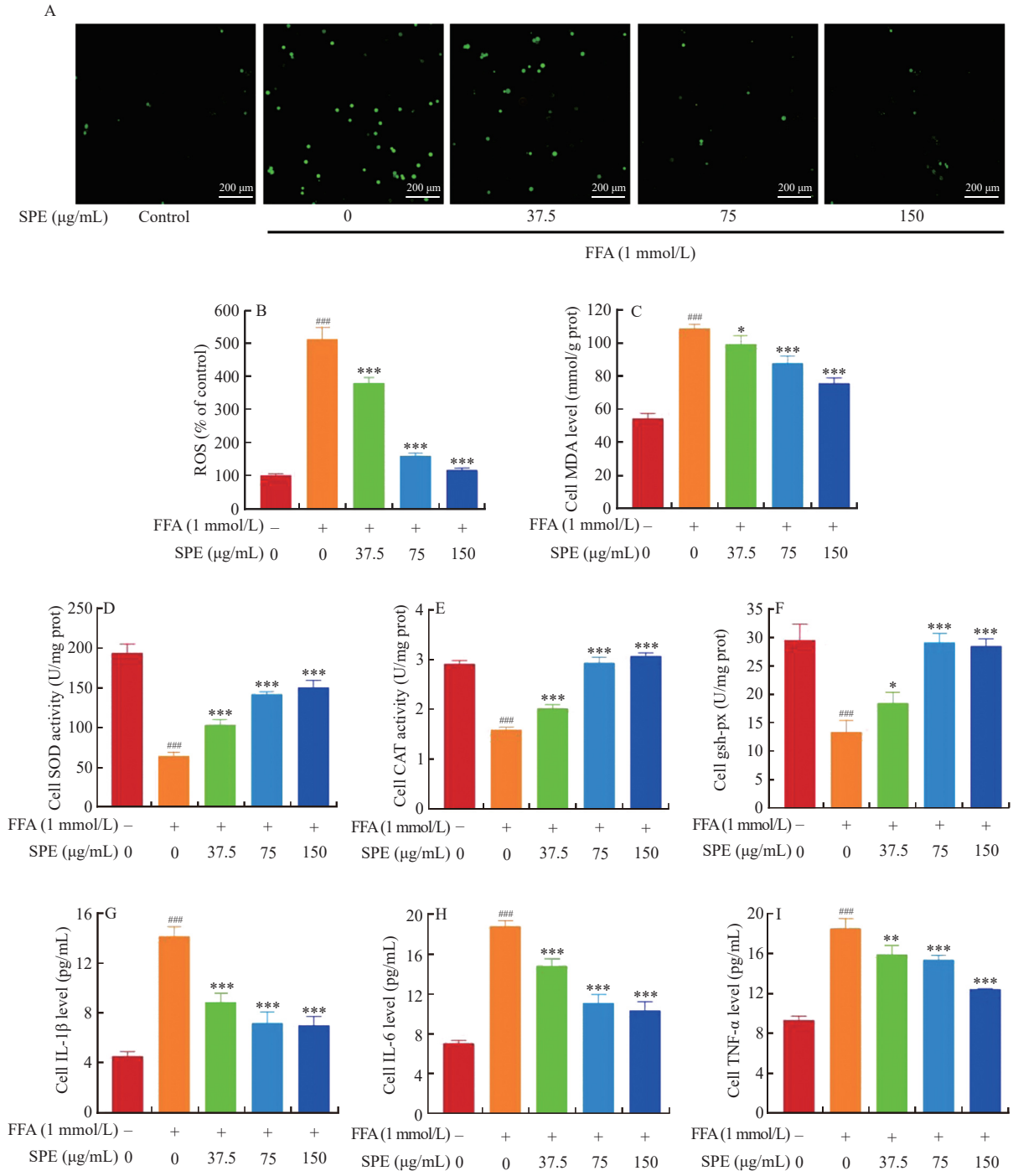

Fig. 3 SPE suppressed oxidative stress and inflammation in FFA-induced HepG2 cells. (A) Cells ROS fluorescent staining. (B) Quantitative analysis of cells fluorescent staining. (C) Cells MDA level. (D) Cells SOD activity. (E) Cells CAT activity. (F) Cells GSH-Px activity. (G) Cells IL-1β level. (H) Cells IL-6 level. (I) Cells TNF-α level. Data were presented as the mean ± SEM ($n = 6$). $^{###}P < 0.001$ *vs*. control group; $^{*}P < 0.05$, $^{**}P < 0.01$, and $^{***}P < 0.001$ *vs*. FFA group.

12 weeks of HC treatment, mice in MOD group displayed extensive inflammatory cell infiltration, hepatocellular ballooning, and steatosis. Furthermore, ORO staining showed a large amount of fat droplet aggregation in the MOD group (Fig. 5B). NAS was used to assess the histological liver injury. Consistently, NAS were significantly higher in the MOD group than that of the CON group (Fig. 5C, $P < 0.001$). It was evident that SPE notably prevented the exacerbation of hepatic steatosis and lipid accumulation at various degrees. In particular, the SPE group had fewer lipid droplets than the positive drug group (Fig. 5A and B). The results were also consistent with a significantly lower in the NAS score compared with the MOD group (Fig. 5C). Moreover, the levels of serum AST and ALT in MOD group ((76.932 ± 3.976), (45.929 ± 2.727) U/L) were significantly higher than that of CON group ((21.335 ± 4.029), (16.559 ± 3.948) U/L; $P < 0.001$). It is well-known that the AST and ALT are 2 key enzymes in liver cells. The AST is mainly presented in the myocardium and liver, while ALT is mainly found in the liver. When the liver is damaged, the 2 enzymes are released into the blood, resulting in increased

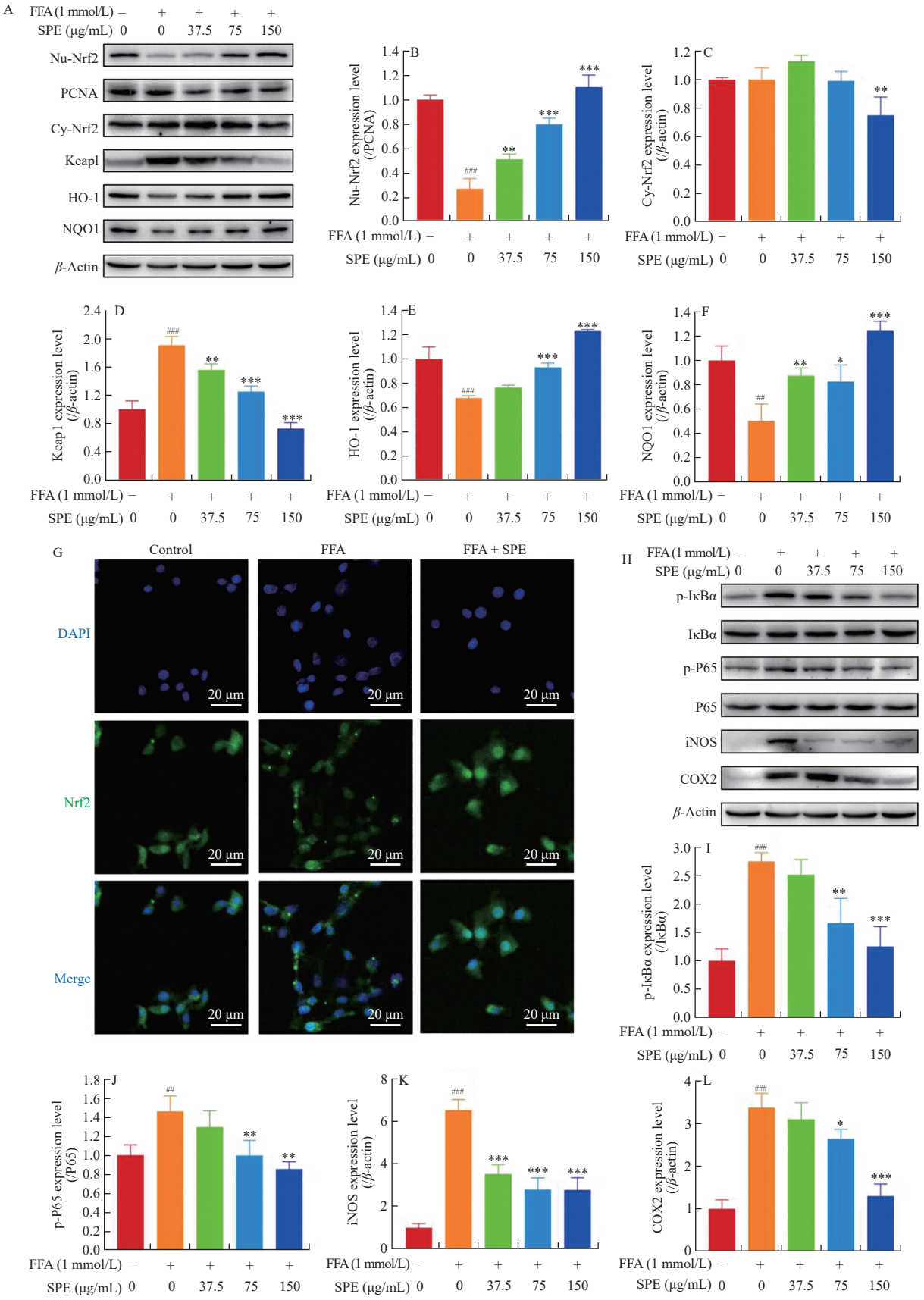

Fig. 4 SPE regulated Nrf2/HO-1 and IκBα/NF-κB pathway in FFA-induced HepG2 cells. (A-F) The protein expression level of Nu-Nrf2, Cy-Nrf2, Keap1, HO-1 and NQO1 in HepG2 cells, as well as the quantification values of these stripes. (G) Expression of Nrf2 in cells detected *via* immunofluorescence analysis. (H-L) Protein expression level of, p-IκBα, p-P65, iNOS and COX2 in HepG2 cells, as well as the quantification values of these stripes. Data were presented as the mean ± SEM ($n = 3$). $^{\#\#}P < 0.01$, $^{\#\#\#}P < 0.001$ *vs*. control group; $^{*}P < 0.05$, $^{**}P < 0.01$, and $^{***}P < 0.001$ *vs*. FFA group.

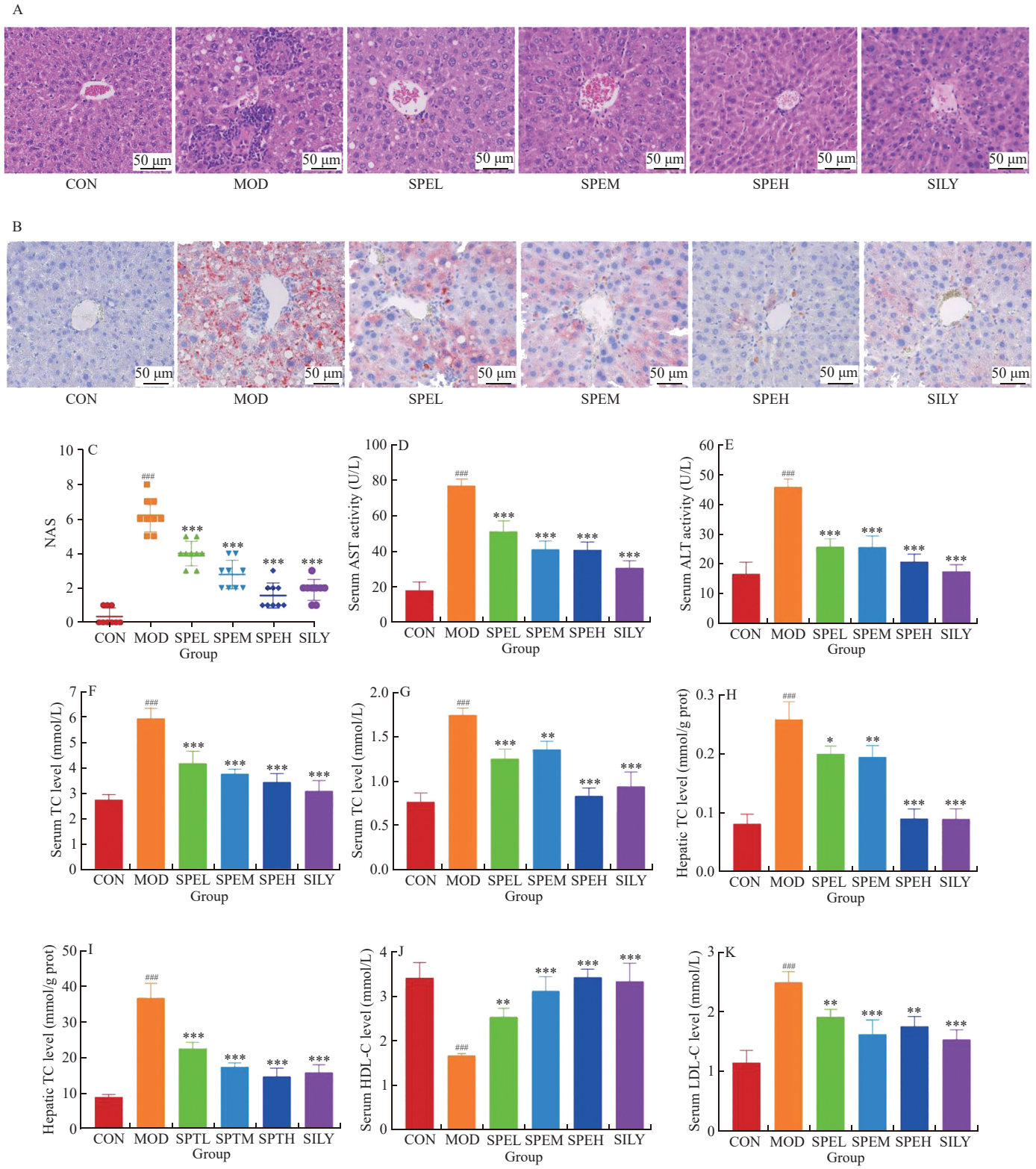

Fig. 5 SPE ameliorated liver injury and steatosis in HC-induced mice. (A) H&E staining in liver tissue. (B) ORO staining in liver tissue. (C) The double-blind evaluation of the liver pathological damage using the NAS system. (D) Serum AST activity. (E) Serum ALT activity. (F) Serum TG level. (G) Serum TC level. (H) Hepatic TG level. (I) Hepatic TC level. (J) Serum HDL-C level. (K) Serum LDL-C level. Data were presented as the mean ± SEM ($n = 6$). ### $P < 0.001$ *vs*. CON group; *$P < 0.05$, ** $P < 0.01$, and *** $P < 0.001$ *vs*. MOD group.

levels of AST and ALT in the blood[31]. However, the serum AST and ALT significantly decreased in dose-dependent manners in treatment groups with SPE (Figs. 5D and F). The levels of serum and hepatic TG and TC in MOD group were higher than those in the CON group. It could be found that the levels of SPEH group were significantly lower compared with the MOD group ($P < 0.001$). Especially, the serum TG

levels in the SPEH group ((0.831 ± 0.090) mmol/L) were close to those observed in the CON group ((0.765 ± 0.101) mmol/L) and less than SILY group ((0.938 ± 0.164) mmol/L). Similarly, the level of HDL-C decreased in HC treated mice, but increased in SPE and silymarin treated mice, and the levels of LDL-C in SPE and SILY groups were higher than those in MOD group. These results indicated that SPE had hepatic protective effects against HC-induced liver injury and steatosis.

3.7 SPE relieved oxidative stress and inflammation in HC-induced mice

To investigate the effects of SPE on oxidative stress in HC-induced mice, the oxidative stress markers levels in serum and liver tissues were measured and shown in Tables 1 and 2. The MDA was the product of lipid peroxidation, and the results showed that mice treated with HC caused a significant increase on MDA levels of serum and liver ((17.658 ± 0.899) nmol/mL, (3.149 ± 0.095) nmol/mg prot). However, the MDA levels remarkably decreased in SPE treatment group (Tables 1 and 2). Contents of MDA in serum and liver from the SPEH group were line with those in the CON group. Meanwhile, modern investigations indicated that the oxidative stress has been related in the pathogenesis and progression of NASH[32]. Therefore, the enzyme activity levels of SOD, CAT and GSH-Px were used to evaluate the efficacy of plant extract[33]. Additionally, HC treatment decrease the levels of SOD, CAT and GSH-Px both in serum and liver ($P < 0.001$). SPE and silymarin treatment groups significantly increased the antioxidant enzymes activity (Tables 1 and 2). Moreover, the levels of T-AOC in serum and liver were dramatically reduced in MOD group ((0.191 ± 0.022) mmol TE/mL, (0.197 ± 0.009) mmol TE/mg prot; $P < 0.001$). However, SPE administration reversed this trend in a dose-dependent manner (Tables 1 and 2). Studies have shown that persistent oxidative stress led to inflammation. Therefore, we detected the levels of pro-inflammatory cytokines, including IL-1β, IL-6 and TNF-α in each group. The results showed the SPE markedly reversed the elevation in IL-1β, IL-6 and TNF-α (Figs. 6A-F). The levels of serum and liver pro-inflammatory cytokines in the SPEM and SPEH groups were comparable to those in the SILY group. In particular, the level of hepatic TNF-α in SPEM and SPEH groups ((14.925 ± 2.474), (13.516 ± 2.205) ng/g tissue) were lower than SILY group ((16.323 ± 2.458) ng/g tissue; Fig. 6F). Above results suggested the SPE could relieve oxidative stress and inflammation mice HC-induced.

3.8 SPE mitigated liver fibrosis in HC-induced mice

Fibrosis was considered to be a typical marker of NASH progression[1]. To further investigate the effect of SPE on HC-induced liver fibrosis in mice, liver sections were stained with Sirius red and Masson. The micrograph of Sirius red and Masson staining displayed an abundant distribution of collagen in the hepatic vein after HC treatment in MOD group. The SPE alleviated liver fibrosis and the therapeutic effect at a dose of 1 000 mg/kg in SPEH group was close to the CON groups. However, SILY group showed less change than SPEH group (Figs. 6G-H). Hydroxyproline (HYP) and Col-I were identified as indicators for evaluating hepatic fibrosis level. The HYP and Col-I levels of liver in MOD group mice ((0.565 ± 0.042) μg/g tissue, (54.135 ± 6.890) ng/g tissue) were remarkably increased compared with the CON group ((0.312 ± 0.033), (19.627 ± 2.125) ng/g tissue). SPE decreased the levels of liver HYP and Col-I dose-dependently and the Col-I level in SPEH group ((30.687 ± 4.302) ng/g tissue) was lower than SILY group ((33.997 ± 5.109) ng/g tissue, Figs. 6I-J). These results indicated that SPE suppressed the progression of the fibrosis.

Table 1
SPE increased the levels of antioxidant enzymes in serum.

Group	MDA (nmol/mL)	SOD (U/mL)	CAT (U/mL)	GSH-Px (U/mL)	T-AOC (mmol TE/mL)
CON	6.667 ± 0.680	229.744 ± 15.115	3.197 ± 0.196	176.417 ± 23.022	0.471 ± 0.030
MOD	17.658 ± 0.899$^{\#\#\#}$	114.647 ± 14.426$^{\#\#\#}$	1.546 ± 0.107$^{\#\#\#}$	83.900 ± 21.354$^{\#\#\#}$	0.191 ± 0.022$^{\#\#\#}$
SPEL	12.072 ± 2.433**	185.904 ± 15.346***	1.812 ± 0.100	106.576 ± 11.887	0.278 ± 0.035*
SPEM	8.243 ± 1.331***	189.839 ± 6.373***	2.414 ± 0.199***	152.381 ± 9.527***	0.294 ± 0.011**
SPEH	8.063 ± 0.858***	197.117 ± 24.738***	2.886 ± 0.152***	176.417 ± 5.151***	0.383 ± 0.049***
SILY	6.532 ± 1.226***	208.812 ± 6.900***	2.620 ± 0.196***	190.476 ± 7.575***	0.434 ± 0.030***

Note: Data were presented as the mean ± SEM ($n = 6$). $^{\#}P < 0.05$, $^{\#\#}P < 0.01$, and $^{\#\#\#}P < 0.001$ *vs*. CON group; *$P < 0.05$, **$P < 0.01$, and ***$P < 0.001$ *vs*. MOD group.

Table 2
SPE increased the levels of antioxidant enzymes in liver.

Group	MDA (nmol/mg prot)	SOD (U/mg prot)	CAT (U/mg prot)	GSH-Px (U/mg prot)	T-AOC (U/mg prot)
CON	1.207 ± 0.068	229.607 ± 22.208	8.100 ± 0.748	309.297 ± 11.410	0.603 ± 0.040
MOD	3.149 ± 0.095$^{\#\#\#}$	139.933 ± 13.244$^{\#\#\#}$	4.637 ± 0.446$^{\#\#\#}$	93.878 ± 10.272$^{\#\#\#}$	0.197 ± 0.009$^{\#\#\#}$
SPEL	1.883 ± 0.108***	142.680 ± 11.002	6.293 ± 0.649*	171.429 ± 21.598***	0.373 ± 0.010***
SPEM	1.905 ± 0.146***	192.919 ± 16.449**	7.001 ± 0.476**	238.549 ± 20.827***	0.393 ± 0.021***
SPEH	1.757 ± 0.059***	215.917 ± 24.865***	6.971 ± 0.434***	247.166 ± 11.081***	0.386 ± 0.033***
SILY	1.572 ± 0.135***	226.645 ± 16.527***	8.296 ± 0.969***	315.193 ± 10.568***	0.507 ± 0.020***

Note: Data were presented as the mean ± SEM ($n = 6$). $^{\#}P < 0.05$, $^{\#\#}P < 0.01$, and $^{\#\#\#}P < 0.001$ *vs*. CON group; *$P < 0.05$, **$P < 0.01$, and ***$P < 0.001$ *vs*. MOD group.

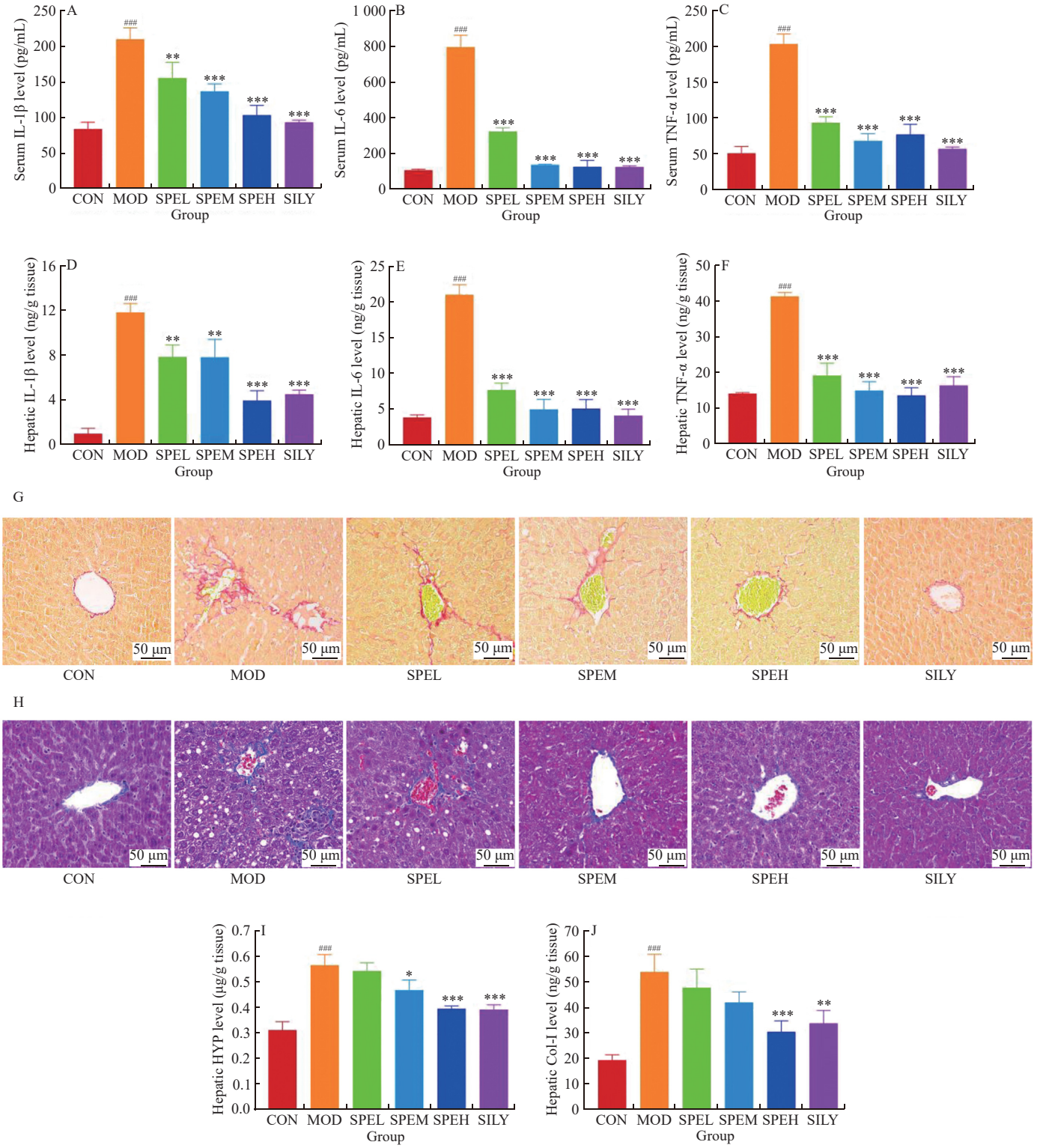

Fig. 6 SPE relieved inflammation and fibrosis in HC-induced mice. (A) Serum IL-1β level. (B) Serum IL-6 level. (C) Serum TNF-α level. (D) Hepatic IL-1β level. (E) Hepatic IL-6 level. (F) Hepatic TNF-α level. (G) Sirius red staining in liver tissue Serum. (H) Masson staining in liver tissue. (I) Hepatic Col-I level. (J) Hepatic HYP level. Data were presented as the mean ± SEM (n = 6). $^{###}P < 0.001$ *vs*. CON group; $^{*}P < 0.05$, $^{**}P < 0.01$, and $^{***}P < 0.001$ *vs*. MOD group.

3.9 SPE regulated Nrf2 and NF-κB pathways in HC-induced NASH mice

To prove the underlying mechanism of SPE on inflammation and oxidative stress *in vivo*, the Nrf2 and NF-κB pathways related proteins were investigated. The Western blot results showed the SPE dramatically decreased the expression level of Keap1 compared to MOD group ($P < 0.001$, Figs. 7A and D). Thus, the expression of nuclear Nrf2 (Nu-Nrf2) was markedly enhanced by the employment of SPE (Figs. 7A-C). Consistently, the downstream

target proteins HO-1 and NQO1 were declined in MOD group, while SPE administration reversed the decrease in a dose-dependent manner and the levels of HO-1 and NQO1 in the SPEH group were comparable with the CON group (Figs. 7A, E and F). Meanwhile, the expression of inflammation related proteins p-IκBα and p-P65 were significantly increased in MOD group. After gavage with SPE, the levels of p-IκBα and p-P65 were decreased in a dose-dependent manner. In particular, the level of p-P65 in SPEH and SILY groups were lower than that of the CON group (Figs. 7G-I). These results illustrated that SPE protected liver from oxidative stress and inflammation through regulating Nrf2 and NF- κB signaling pathways.

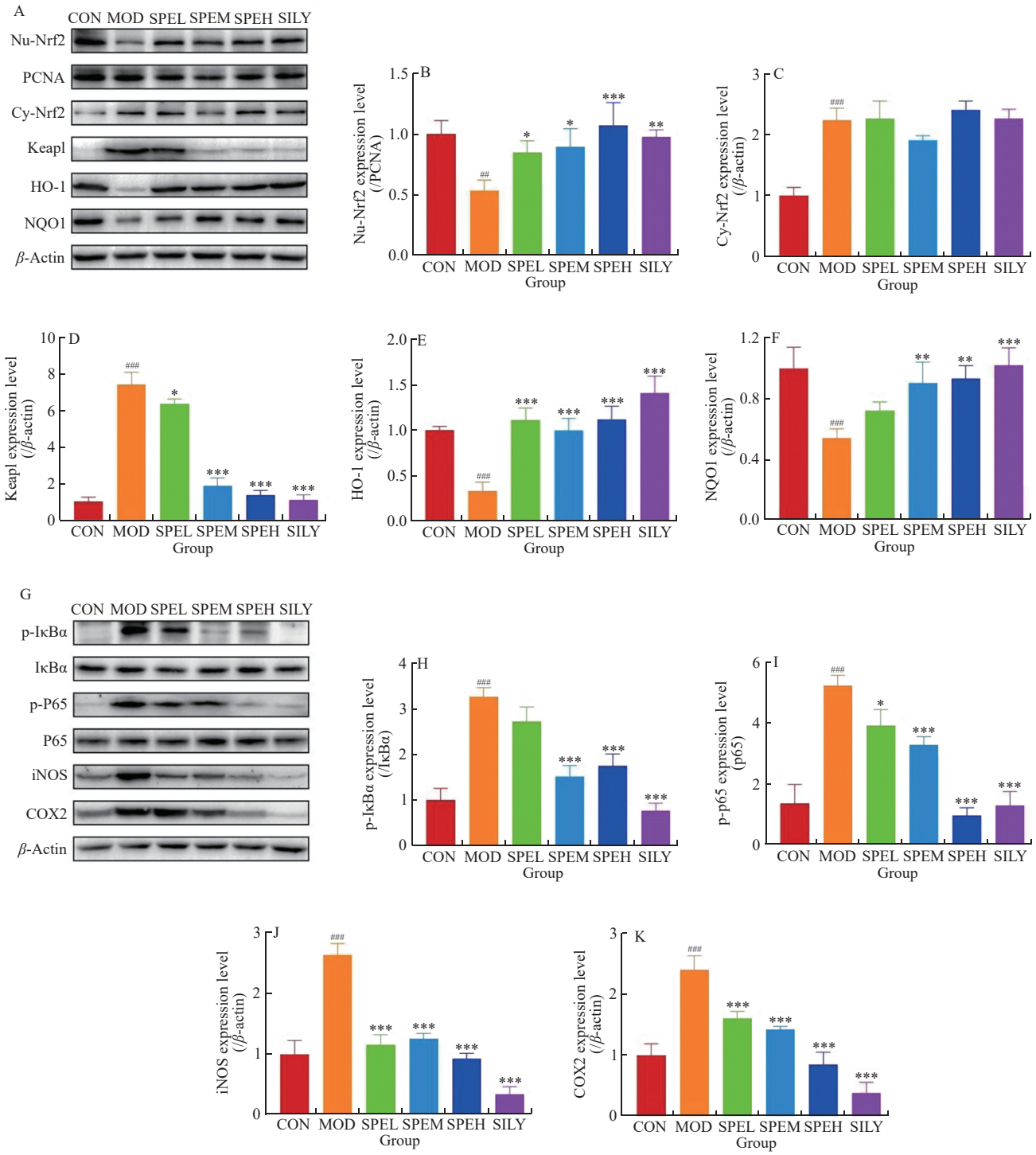

Fig. 7 SPE regulated Nrf2/HO-1 and IκBα/NF-κB pathway in HC-induced NASH mice. (A-F) The protein expression level of Nu-Nrf2, Cy-Nrf2, Keap1, HO-1 and NQO1 in mice, as well as the quantification values of these stripes. (G-K) The protein expression level of p-IκBα, p-P65, iNOS and COX2 in mice, as well as the quantification values of these stripes. Data were presented as the mean ± SEM ($n = 3$). $^{\#\#}P < 0.001$, $^{\#\#\#}P < 0.001$ *vs*. CON group; $^{*}P < 0.05$, $^{**}P < 0.01$, and $^{***}P < 0.001$ *vs*. MOD group.

3.10 SPE regulated TGF-β1 pathway in HC-induced NASH mice

To explore the potential mechanism of SPE in inhibiting liver fibrosis, the relative proteins TGF-β1, Smad2 and α-SMA were detected. As shown in Figs. 8A and B, the level of TGF-β1 expression in liver tissues was markedly increased in MOD group and evidently decreased in SPE groups. Similarly, after the treatment with HC, the expressions of p-Smad2 stimulated by TGF-β1 were lifted. After 6-weeks of feeding with SPE, the level of p-Smad2 was reduced in a dose-dependent manner. Moreover, the degree of Smad2 phosphorylation in SPE treatment was comparable to that of the CON group (Figs. 8A and C). In addition, SPE decreased the elevation of α-SMA by HC and the level of α-SMA in SPEH was less than SILY group (Fig. 8A and D). These results showed that SPE inhibited liver fibrosis through downregulating TGF-β1 pathway.

3.11 Molecular docking analysis

To further elucidate the underlying mechanism of SPE on HC-induced mice, each of the 7 bioactive glycosides was made to interact with each of the 5 protein structures (Keap1, NF-κB, TGF-β1, Smad2, α-SMA). In total, 35 protein-ligand complexes with 7 binding structures per protein were found. The bind energy of complexes was showed in Table S3. The results illustrated Keap1 had the largest number of complexes with low binding energy (< 6 kcal/mol), followed by TGF-β1. According to binding energy, 4 protein-ligand complexes (Keap1-isoacteoside, Keap1-salidroside, Keap1-oleuropein, TGF-β-verbascoside) were selected and analyzed molecule interacting to protein as shown in Table S4. The results indicated that isoacteoside, salidroside and oleuropein entered the binding pocket of Keap1 and the free energy of binding was –8.31, –8.08 and –7.82 kcal/mol, respectively. Verbascoside bound to active site of TGF-β and the energy was –7.94 kcal/mol.

The most possible interaction modes of the 4 complexes were shown in Figs. S2A-D. Previous studies have reported that the Keap1 binding pocket residues Tyr334, Arg380, Asn382, Arg415, Arg483, Tyr525 and Tyr572 connected the Neh2 domain of Nrf2 and their substitutions impaired Keap1 binding to Nrf2[34]. The molecular docking revealed that isoacteoside interacted with the 5 residues mentioned above, 2 of them formed hydrogen bonds while Arg380 formed a stable structure through π-cation interaction. Moreover, Tyr525 and Tyr572 formed a hydrophobic interaction with isoacteoside (Table S4, Fig. S2A). The Keap1-salidroside complex illustrated that salidroside interacted with Arg415 in the above residues and formed hydrogen bond and salt bridge (Table S4, Fig. S2B). Similarly, oleuropein interacted with 5 residues of Keap1, Arg380, Asn382, Arg415 and Tyr525 involved hydrogen bonding while Arg415 and Arg483 formed salt bridge (Table S4, Fig. S2C). TGF-β1 have a Y-type binding pocket as an important structural feature[35]. As shown in Fig. S2D, TGF-β1 residues such as Ile211, Leu260 and Ala350 formed a hydrophobic cavity, and the Y-shaped glycosides verbascoside extended into the cavity to form a stable structure through hydrophobic interaction. In the meantime, a salt bridge was formed between the residue Lys232 and the ligand. There were other 6 residues from TGF-β form hydrogen bonds with verbascoside. Molecular docking analysis showed that the bioactive glycosides in SPE had a high number of interactions with Keap1 and TGF-β, especially isoacteoside, salidroside, oleuropein and verbascoside.

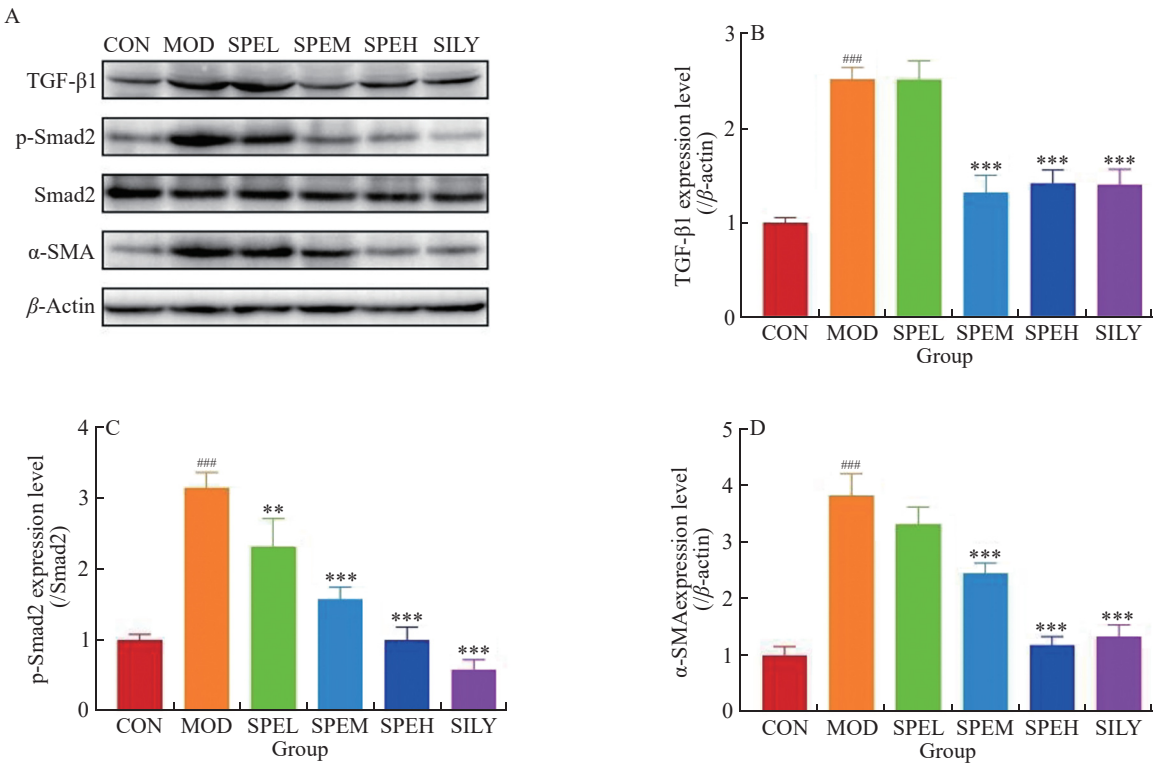

Fig. 8 SPE regulated TGF-β1/Smad2 pathway in HC-induced NASH mice. (A-D) The protein expression level of TGF-β1, p-Smad2 and α-SMA in mice, as well as the quantification values of these stripes. Data were presented as the mean ± SEM ($n = 3$). $^{###}P < 0.001$ *vs*. CON group; $^{***}P < 0.001$ *vs*. MOD group.

4. Discussion

NASH, an aggressive form of NAFLD, which is one of the consequences of the Western lifestyle and HFD and become a prevalent global chronic liver disease[36]. NASH is characterized by the accumulation of lipids and the imbalance of oxidation-antioxidant state in the liver[37]. Numerous medical treatments are being tested in clinical trials[38-39]. However, there is no approved effective therapy for NASH. At present, the general practical approaches to NASH patients are to change HFD and incorporate with weight loss medications to lose total body weight[40]. Therefore, safe and effective approaches are needed to prevent this disease. SP, due to its biological activities and economic value, has been used as healthcare food and food supplies for a long time in Chinese folk[41]. In this study, the improvement effect of SPE on NASH *in vitro* and *in vivo* were evaluated. The results demonstrated that SPE possessed comprehensive ameliorative effect on NASH.

Glycosides are widely distributed in various phytomedicines and have been extensively studied for their potent biological activities[42]. Wang et al.[23] identified 6 glycosides including salidroside, echinacoisde, forsythoside B, verbascoside, isoacteoside and oleuropein from SP and found the glycosides had antioxidant activities *in vitro*. In this study, a novel glycoside, syringoside, was identified in SPE for the first time. Furtherly, FFA-induced HepG2 cells was used to investigate the ameliorative effect of SPE on NASH *in vitro*[43]. As SPE exhibited no cytotoxicity on HepG2 cells at concentrations below 600 μg/mL, the dose at 37.5, 75.0, 150.0 μg/mL were selected for the experiments *in vitro*. The results showed that SPE dropped the lipid profile, attenuated the oxidative stress and inflammation in FFA-induced HepG2 cells. Especially at the concentration of 150 μg/mL, SPE had a remarkable effect in improving oxidative stress and inflammation.

The NASH animal model is induced by HFD, which causes similar features to human NASH. Nevertheless, standard HFD generally does not induce severe steatosis and fibrosis, the significant characteristic for human NASH[44-45]. Tsuchida et al.[46] established an ideal animal NASH model by a combination of HFD and CCl_4. To investigate the effect of SPE on NASH, the mice NASH models induced by HFD combined with weekly CCl_4 intraperitoneal injection were established. The results revealed that chronic HFD feeding combined with CCl_4 injection increased the levels of serum AST, ALT, TG, TC, HDL-C and LDL-C, which were markers of liver injury and lipid accumulation. The indices were significantly decreased after SPE treatment. Silymarin is widely used as positive control drug for *in vivo* studies due to its significant therapeutic effects on liver diseases[47-48]. In the present study, SPE at 1 000 mg/kg had the equal or slightly higher effects than silymarin on lipid accumulation and liver injury in HC-induced NASH mice.

During the development of NASH, oxidative stress plays an important role[5,49]. Protecting the organism from the damages of oxidative stress is a complex system of antioxidant enzymes including SOD, CAT and GSH-Px[50]. A growing number of studies have suggested that the levels of hepatic MDA and ROS are sharply raised in patients with NASH, and the levels of antioxidant enzymes are significantly declined[51-52]. Not surprisingly, the results in this study revealed that the levels of MDA and ROS were notably increased both in FFA-treated cells and HC-induced mice, and SPE administration reduced the over-production. In addition, the results revealed that the levels of SOD, CAT and GSH-Px were decreased in NASH model *in vitro* and *in vivo* and the activity of these antioxidant enzymes increased after SPE treatment. Interestingly, these antioxidant enzymes are closely related to Nrf2, a crucial pathway protein for protecting hepatocytes from oxidative stress[53]. During the progression of NASH, Nrf2 is down-regulated and the levels of antioxidant enzymes are descended which accelerates the disease, whereas the upregulation of Nrf2 suppresses NASH[54]. Keap1 is a major negative regulator of Nrf2, which mediates the ubiquitination of Nrf2 in cell[55]. Manifold researches showed the repression of Keap1 could increase Nrf2 activity[56]. In present study, the SPE decreased the level of Keap1 while increased the level of nuclear Nrf2 compared to NASH model *in vitro* and *in vivo*. The results of immunofluorescence assay suggested that Nrf2 was transferred from cytoplasm to nucleus. Meanwhile, the levels of downstream proteins HO-1 and NQO1 were raised by SPE treatment. Molecular docking revealed the possible pattern of SPE repressing Keap1 and activating Nrf2. The β propeller structure is a characteristic of Keap1 and its integrity effectively represses Nrf2 activity[57]. Hong et al.[58] demonstrated that there was strong binding affinity between Keap1 and echinacoside, forsythoside B, isoacteoside and salidroside *via* molecular docking. In this study, the results discovered that 7 glycosides of SPE including echinacoside, forsythoside B, isoacteoside, oleuropein, salidroside, syringoside, and verbascoside interacted with residues of the β propeller structure in Keap1 and effectively relieved inhibitory effect of Keap1 on Nrf2, which enhanced the expression of Nrf2 and downstream proteins.

Previous researches revealed the continued oxidative stress could lead to chronic inflammation and the proinflammatory cytokines will raise[59]. Similarly, this study showed the levels of IL-1β, IL-6 and TNF-α were enhanced in FFA-treated cells and HC-induced mice, and SPE employment down-regulated this tendency. The pro-inflammatory cytokines were mediated by NF-κB. Previous researches showed that IκBα was activated and then caused NF-κB p65 phosphorylation in NASH[60]. In this study, SPE administration attenuated the phosphorylation of IκBα and NF-κB p65. Meantime, the levels of inflammation-related enzymes including iNOS and COX-2 were decreased. Notably, recent studies have confirmed a correlation between Nrf2 and NF-κB pathways and revealed that Nrf2 inhibited the phosphorylation and nuclear translocation of NF-κB[61]. Molecular docking results in this study showed that SPE glycosides bind well to NF-κB but with less binding energy than Keap1 complexes. Thus, the current study suggested the ameliorative effect of SPE on inflammation in NASH was closely related to Nrf2 antagonism of NF-κB.

Many investigations revealed that the liver inflammation further activate the fibrotic[6]. Liver fibrosis is considered to be a critical pathological feature of NASH in the past decade[62]. TGF-β1 is the key mediator in the progression of fibrosis. Previous studies proved the generation of TGF-β1 phosphorylate Smad2 and Smad3, which increased the expression of downstream proteins α-SMA and Col-I in NASH. And there was a correlation between above gene expression and liver HYP content[63]. As expected, the present study showed that SPE significantly down-regulated the expression level of TGF-β1 and inhibited the phosphorylation of Smad2 in liver tissue. Correspondingly, the level of α-SMA, HYP and Col-I were decreased. Eventually, Sirius red staining of liver tissues showed the fibrosis was reduced. Furthermore, molecular docking revealed the underlining mechanism of the inhibitory effect of SPE on TGF-β1. The crystal structure showed TGF-β1 possessed a natural Y-type binding pocket and most glycosides of SPE binding to this site with low energy, especially verbascoside. To our knowledge, this is the first time to report molecular docking crystal structure between verbascoside and TGF-β1.

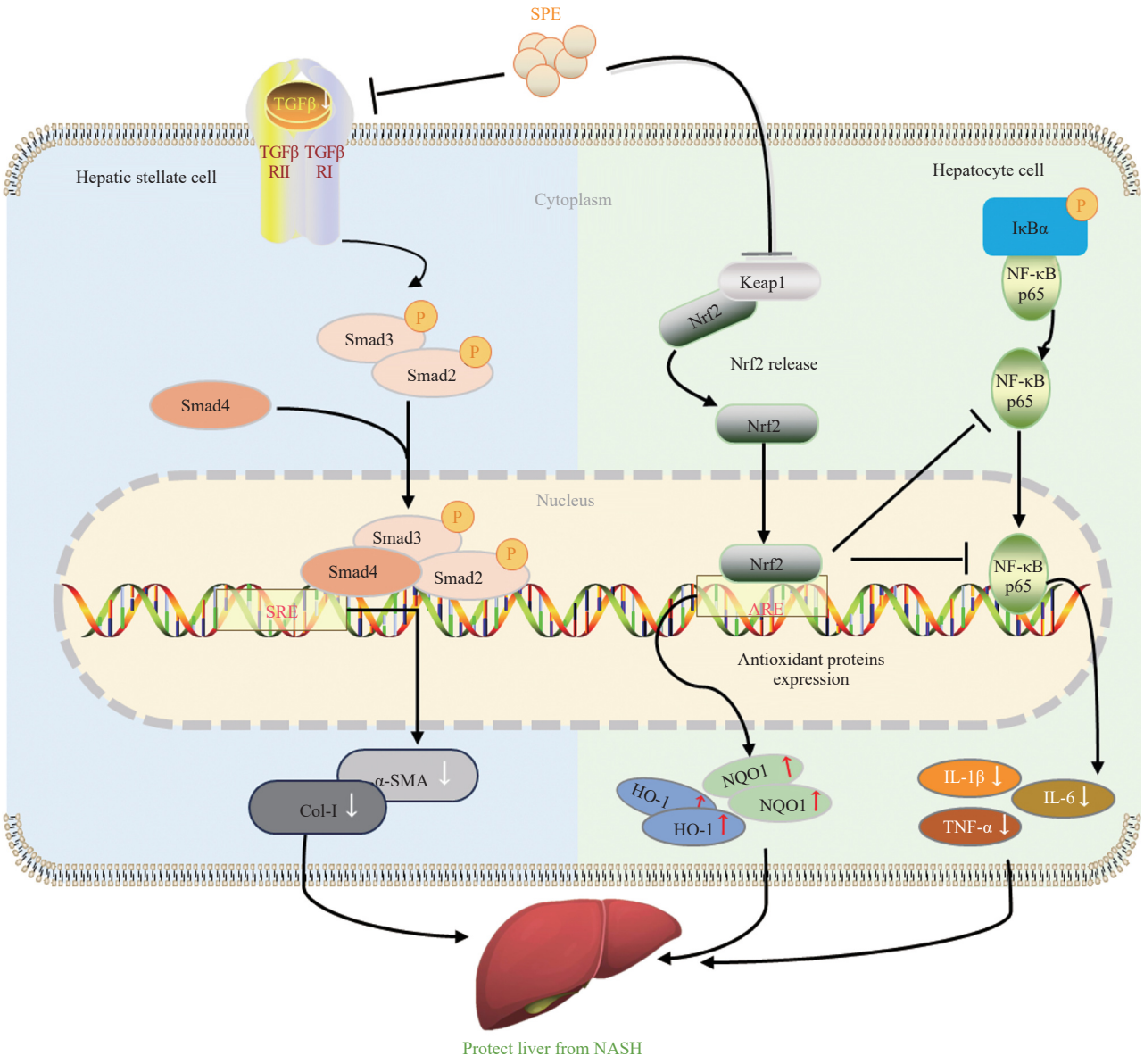

Fig. 9 SPE improves NASH *via* the Nrf2, NF-κB and TGF-β1 signaling pathways.

5. Conclusion

In this study, the efficacy of SPE in improving NASH was comprehensively evaluated and the results demonstrated that SPE alleviated lipid accumulation, oxidative stress, inflammation and fibrosis by regulating Nrf2, IκBα and TGF-β1 pathways in the progression of NASH (Fig. 9). In summary, this study showed that SPE had the potential to be a novel food supplement for the improvement of NASH.

Conflict of interest

The authors declare that they have no known competing financial interests or personal relationships that could have appeared to influence the work reported in this paper.

Acknowledgements

This research is supported by grants from the National Natural Science Foundation of China (U1804175, 32270418), the Joint Fund of Provincial Science and Technology Research and Development plan of Henan Province (232103810055, 232301420100).

Data availability

The data in this study are available from the corresponding author on reasonable request.

Appendix A. Supplementary information

Supplementary data associated with this article can be found, in the online version, at http://doi.org/10.26599/FSHW.2024.9250244.

References

[1] S.R. Wesolowski, K.C.E. Kasmi, K.R. Jonscher, et al., Developmental origins of NAFLD: a womb with a clue, Nat. Rev. Gastr. Hepat. 14 (2016) 81-96. https://doi.org/10.1038/nrgastro.2016.160.

[2] E.E. Powell, V.W.S. Wong, M. Rinella, Non-alcoholic fatty liver disease, Lancet 397 (2021) 2212-2224. https://doi.org/10.1016/s0140-6736(20)32511-3.

[3] A.C. Sheka, O. Adeyi, J. Thompson, et al., Nonalcoholic steatohepatitis: a review, JAMA 323 (2020) 1175-1183. https://doi.org/10.1001/jama.2020.2298.

[4] G. Musso, M. Cassader, R. Gambino, Non-alcoholic steatohepatitis: emerging molecular targets and therapeutic strategies, Nat. Rev. Drug Discov. 15 (2016) 249-274. https://doi.org/10.1038/nrd.2015.3.

[5] Z. Ke, Y. Zhao, S. Tan, et al., *Citrus reticulata* Blanco peel extract ameliorates hepatic steatosis, oxidative stress and inflammation in HF and MCD diet-induced NASH C57BL/6 J mice, J. Nutr. Biochem. 83 (2020) 108426. https://doi.org/10.1016/j.jnutbio.2020.108426.

[6] Y. Koyama, D.A. Brenner, Liver inflammation and fibrosis, J. Clin. Invest. 127 (2017) 55-64. https://doi.org/10.1172/JCI88881.

[7] M. Qiu, F. Xiao, T. Wang, et al., Protective effect of Hedansanqi Tiaozhi Tang against non-alcoholic fatty liver disease *in vitro* and *in vivo* through activating Nrf2/HO-1 antioxidant signaling pathway, Phytomedicine 67 (2020) 153140. https://doi.org/10.1016/j.phymed.2019.153140.

[8] T. Nguyen, P. Nioi, C.B. Pickett, The Nrf2-antioxidant response element signaling pathway and its activation by oxidative stress, J. Biol. Chem. 284 (2009) 13291-13295. https://doi.org/10.1074/jbc.R900010200.

[9] S.M. Ahmed, L. Luo, A. Namani, et al., Nrf2 signaling pathway: pivotal roles in inflammation, Biochim. Biophys. Acta. Mol. Basis. Dis. 1863 (2017) 585-597 https://doi.org/10.1016/j.bbadis.2016.11.005.

[10] M. Sandberg, J. Patil, B. D'Angelo, et al., NRF2-regulation in brain health and disease: implication of cerebral inflammation, Neuropharmaco. 79 (2014) 298-306. https://doi.org/10.1016/j.neuropharm.2013.11.004.

[11] U. Moens, S. Kostenko, B. Sveinbjornsson, The role of mitogen-activated protein kinase-activated protein kinases (MAPKAPKs) in inflammation, Genes 4 (2013) 101-133. https://doi.org/10.3390/genes4020101.

[12] X.M. Meng, D.J. Nikolic-Paterson, H.Y. Lan, TGF-β: the master regulator of fibrosis, Nat. Rev. Nephro. 12 (2016) 325-338. https://doi.org/10.1038/nrneph.2016.48.

[13] F. Xu, C. Liu, D. Zhou, et al., TGF-β/SMAD pathway and its regulation in hepatic fibrosis, J Histochem. Cytochem. 64 (2016) 157-167. https://doi.org/10.1369/0022155415627681.

[14] A.M. Oseini, A.J. Sanyal, Therapies in non-alcoholic steatohepatitis (NASH), Liver In. 37 (2017) 97-103. https://doi.org/10.1111/liv.13302.

[15] M.J. Armstrong, P. Gaunt, G.P. Aithal, et al., Liraglutide safety and efficacy in patients with non-alcoholic steatohepatitis (LEAN): a multicentre, double-blind, randomised, placebo-controlled phase 2 study, Lancet 387 (2016) 679-690. https://doi.org/10.1016/s0140-6736(15)00803-x.

[16] R. Loomba, Z. Kayali, M. Noureddin, et al., GS-0976 reduces hepatic steatosis and fibrosis markers in patients with nonalcoholic fatty liver disease, Gastroenterol. 155 (2018) 1463-1473. https://doi.org/10.1053/j.gastro.2018.07.027.

[17] H. Xu, Q. Zhao, N. Song, et al., AdipoR1/AdipoR2 dual agonist recovers nonalcoholic steatohepatitis and related fibrosis *via* endoplasmic reticulum-mitochondria axis, Nat. Commun. 11 (2020) 5807. https://doi.org/10.1038/s41467-020-19668-y.

[18] S. Wang, L. Yang, A. Hou, et al., Screening hepatoprotective effective components of *Lonicerae japonica* Flos based on the spectrum-effect relationship and its mechanism exploring, Food Sci. Hum. Wellness 12 (2023) 283-294. https://doi.org/10.1016/j.fshw.2022.07.018.

[19] Y.F. Wu, Y.D. Chu, Q.Y. Yang, et al., Response surface methodology optimised solvothermal system enables an efficient extraction of echinacoside and oleuropein from *Syringa pubescens* Turcz, Phytochem. Anal. 32 (2021) 1074-1081 https://doi.org/10.1002/pca.3049.

[20] Y.F. Wu, Q.Y. Yang, D.J. Wang, et al., A comparative study of echinacoside, oleuropein content and antioxidant properties of different solvent extracts from *Syringa pubescens* Turcz, Pak. J. Pharm. Sci. 35 (2022) 33-38. https://doi.org/10.36721/pjps.2022.35.1.Reg.035-040.1.

[21] H. Zhang, Protective effects of *Syringa pubescens* extract on liver injury induced by cadmium in mice, Clin. Res. Pract. 3 (2018) 155-156. https://doi.org/10.19347/j.cnki.2096-1413.201824072.

[22] X.Y. He, J.J. Shi, R.C. Gong, et al., Anti-inflammatory effect of *Syringa pubescens* Turcz., J. Tonghua Norm. Univ. 34 (2013) 55-57. https://doi.org/10.3969/j.issn.1008-7974.2013.12.020.

[23] XS. Wang, JM. Zhang, PX. Wang, et al., Evaluation of alpha-glucosidase inhibition activity and glycosides in the *Syringa pubescens* Turcz from different geographical origin, Sci. Hortic. 320 (2023) 112198. https://doi.org/10.1016/j.scienta.2023.112198.

[24] A.H. Cory, T.C. Owen, J.A. Barltrop, et al., Use of an aqueous soluble tetrazoliumformazan assay for cell growth assays in culture, Cancer Commun. 3 (1991) 207-212. https://doi.org/10.3727/095535491820873191.

[25] Y.A. Xue, Y. Wei, L. Cao, et al. Protective effects of *scutellaria-coptis* herb couple against non-alcoholic steatohepatitis *via* activating NRF2 and FXR pathways *in vivo* and *in vitro*. J. Ethnopharmacol. 318 (2024) 116933. https://doi.org/10.1016/j.jep.2023.116933.

[26] J.M. Zhang, Y.F. Wu, C.Y. Wang, et al., The antioxidant, anti-inflammatory and analgesic activity effect of ethyl acetate extract from the flowers of *Syringa pubescens* Turcz, J. Ethnopharmacol. 322 (2024) 117561. https://doi.org/10.1016/j.jep.2023.117561.

[27] D.E. Kleiner, E.M. Brunt, M. Van Natta, et al., Design and validation of a histological scoring system for nonalcoholic fatty liver disease, Hepatol. 41 (2005) 1313-1321. https://doi.org/10.1002/hep.20701.

[28] X. Shen, W. Zhang, C. Peng, et al., In vitro anti-bacterial activity and network pharmacology analysis of Sanguisorba officinalis L. against Helicobacter pylori infection, Chin. Med. 16 (2021) 33. https://doi.org/10.1186/s13020-021-00442-1.

[29] A. Wu, Z. Yang, Y. Huang, et al., Natural phenylethanoid glycosides isolated from *Callicarpa kwangtungensis* suppressed lipopolysaccharide-mediated inflammatory response *via* activating Keap1/Nrf2/HO-1 pathway in RAW 264.7 macrophages cell, J. Ethnopharmacol. 258 (2020) 112857. https://doi.org/10.1016/j.jep.2020.112857.

[30] S.C. Lo, X. Li, M.T. Henzl, et al., Structure of the Keap1:Nrf2 interface provides mechanistic insight into Nrf2 signaling, EMBO J. 25 (2006) 3605-3617 https://doi.org/10.1038/sj.emboj.7601243.

[31] Y.L. Xu, S. Ting, H. Mishra, et al. Corn oligopeptide alleviates nonalcoholic fatty liver disease by regulating the sirtuin signaling pathway, J. Agric. Food Chem. 72 (2024) 6360-6371. https://doi.org10.1021/acs.jafc.3c09058.

[32] Y.T. Koda, Y.K. Nagasaki. Metabolic dysfunction-associated steatohepatitis treated by poly(ethylene glycol)-block-poly(cysteine) block copolymer-based self-assembling antioxidant nanoparticles, J. Control. Release. 370 (2024) 367-378. https://doi.org/10.1016/j.jconrel.2024.04.050.

[33] C. Cao, C. Chang, Y.Y. Wei, et al. The acute oral toxicity test of ethanol extract of salt-processed *Psoraleae Fructus* and its acute hepatotoxicity and nephrotoxicity risk assessment, J. Ethnopharmacol. 309 (2023) 116334. https://doi.org/10.1016/j.jep.2023.116334.

[34] I.D. Boyenle, U.C. Divine, R. Adeyemi, et al., Direct Keap1-kelch inhibitors as potential drug candidates for oxidative stress-orchestrated diseases: a review on *in silico* perspective, Pharmacol. Res. 167 (2021) 105577. https://doi.org/10.1016/j.phrs.2021.105577.

[35] J.H. Jiang, P. Deng, Discovery of new inhibitors of transforming growth factor-beta type 1 receptor by utilizing docking and structure-activity relationship analysis, Int. J. Mol. Sci. 20 (2019) 4090. https://doi.org/10.3390/ijms20174090.

[36] J.C. Cohen, J.D. Horton, H.H. Hobbs, Human fatty liver disease: old questions and new insights, Science 332 (2011) 1519-1523 https://doi.org/10.1126/science.1204265.

[37] Q. Li, J.X. Tan, Y. He, et al., Atractylenolide III ameliorates Non-alcoholic fatty liver disease by activating hepatic adiponectin receptor 1-mediated AMPK pathway, Int. J. Biol. Sci. 18 (2022) 1594-1611. https://doi.org/10.7150/ijbs.68873.

[38] Y.F Deng, Q.Q. Xu, T.Q. Chen, et al., Kinsenoside alleviates inflammation and fibrosis in experimental NASH mice by suppressing the NF-κB/NLRP3 signaling pathway, Phytomedicine 104 (2022) 154241. https://doi.org/10.1016/j.phymed.2022.154241.

[39] Q.L. Fang, X. Qiao, X.Q. Yin, et al., Flavonoids from *Scutellaria amoena* C. H. Wright alleviate mitochondrial dysfunction and regulate oxidative stress *via* Keap1/Nrf2/HO-1 axis in rats with high-fat diet-induced nonalcoholic steatohepatitis, Biomed. Pharmacother. 158 (2023) 114160. https://doi.org/10.1016/j.biopha.2022.114160.

[40] A. Do, E.J. Kuszewski, K.A. Langberg, et al., Incorporating weight loss medications into hepatology practice for nonalcoholic steatohepatitis, Hepatol. 70 (2019) 1443-1456 https://doi.org/10.1002/hep.30658.

[41] Q.Y. Yang, X.S. Wang, Y.L. Zhang, et al., Simultaneous determination of phenylethanoid glycosides and antioxidant activity of *Syringa pubescens* Turcz. from different geographical origin in China, J. Chromat. Sci. 61 (2023) 766-772. https://doi.org/10.1093/chromsci/bmac099.

[42] X.Y. Fu, Z.J. Sun, Q.Y. Long, et al., Glycosides from Buyang Huanwu Decoction inhibit atherosclerotic inflammation *via* JAK/STAT signaling pathway, Phytomedicine 105 (2022) 154385. https://doi.org/10.1016/j.phymed.2022.154385.

[43] M. Jin, H. Feng, Y. Wang, et al., Gentiopicroside ameliorates oxidative stress and lipid accumulation through nuclear factor erythroid 2-related factor 2 activation, Oxid. Med. Cell. Longevity 2020 (2020) 1-13. https://doi.org/10.1155/2020/2940746.

[44] S.C. Sookoian, M.V. Machado, G.A. Michelotti, et al., Mouse models of diet-induced nonalcoholic steatohepatitis reproduce the heterogeneity of the human disease, Plos One 10 (2015) e0127991. https://doi.org/10.1371/journal.pone.0127991.

[45] S.H. Ibrahim, P. Hirsova, H. Malhi, et al., Animal models of nonalcoholic steatohepatitis: eat, delete, and inflame, Digest. Dis. Sci. 61 (2015) 1325-1336. https://doi.org/10.1007/s10620-015-3977-1.

[46] T. Tsuchida, Y.A. Lee, N. Fujiwara, et al., A simple diet- and chemical-induced murine NASH model with rapid progression of steatohepatitis, fibrosis and liver cancer, J. Hepatol. 69 (2018) 385-395. https://doi.org/10.1016/j.jhep.2018.03.011.

[47] B. Anfuso, P. Giraudi, C. Tiribelli, et al., Silybin modulates collagen turnover in an *in vitro* model of NASH, Molecules 24 (2019) 1280. https://doi.org/10.3390/molecules24071280.

[48] L. Abenavoli, A.A. Izzo, N. Milić, et al., Milk thistle (*Silybum marianum*): a concise overview on its chemistry, pharmacological, and nutraceutical uses in liver diseases, Phytother. Res. 32 (2018) 2202-2213. https://doi.org/10.1002/ptr.6171.

[49] V. Nobili, M. Parola, A. Alisi, et al. Oxidative stress parameters in paediatric non-alcoholic fatty liver disease, Inter. J. Molecul. Med. 26 (2010) 471-476. https://doi.org/10.3892/ijmm_00000487.

[50] H. Sies, Oxidative stress: from basic research to clinical application, Am. J. Med. 91 (1991) 31S-38S. https://doi.org/10.1016/0002-9343(91)90281-2.

[51] L. Polimeni, M.D. Ben, F. Baratta, et al. Oxidative stress: new insights on the association of non-alcoholic fatty liver disease and atherosclerosis, World J. Hepatol. 7 (2015) 1325-1336. https://doi.org/10.4254/wjh.v7.i10.1325.

[52] Y. Kang, Y. Song, Y. Luo, et al., Exosomes derived from human umbilical cord mesenchymal stem cells ameliorate experimental non-alcoholic steatohepatitis *via* Nrf2/NQO-1 pathway, Free Radic. Biol. Med. 192 (2022) 25-36. https://doi.org/10.1016/j.freeradbiomed.2022.08.037.

[53] L.Y. Lee, U.A. Kohler, L. Zhang, et al., Activation of the Nrf2-ARE pathway in hepatocytes protects against steatosis in nutritionally induced non-alcoholic steatohepatitis in mice, Toxicol. Sci. 142 (2014) 361-374. https://doi.org/10.1093/toxsci/kfu184.

[54] B. Bathish, H. Robertson, J.F. Dillon, et al., Nonalcoholic steatohepatitis and mechanisms by which it is ameliorated by activation of the CNC-bZIP transcription factor Nrf2, Free Rad. Biol. Med. 188 (2022) 221-261. https://doi.org/10.1016/j.freeradbiomed.2022.06.226.

[55] A. Kobayashi, M.I. Kang, Y. Watai, et al., Oxidative and electrophilic stresses activate Nrf2 through inhibition of ubiquitination activity of Keap1, Mol. Cell. Biol. 26 (2006) 221-229. https://doi.org/10.1128/MCB.26.1.221-229.2006.

[56] X. Chen, H. Xue, W. Fang, et al., Adropin protects against liver injury in nonalcoholic steatohepatitis *via* the Nrf2 mediated antioxidant capacity, Redox. Biol. 21 (2019) 101068. https://doi.org/10.1016/j.redox.2018.101068.

[57] B. Padmanabhan, K.I. Tong, T. Ohta, et al., Structural basis for defects of Keap1 activity provoked by its point mutations in lung cancer, Molecular Cell 21 (2006) 689-700. https://doi.org/10.1016/j.molcel.2006.01.013.

[58] J. Hong, Z. Shi, C. Li, et al., Virtual screening identified natural Keap1-Nrf2 PPI inhibitor alleviates inflammatory osteoporosis through Nrf2-mir214-Traf3 axis, Free Rad. Biol. Med. 171 (2021) 365-378. https://doi.org/10.1016/j.freeradbiomed.2021.05.020.

[59] S. Reuter, S.C. Gupta, M.M. Chaturvedi, et al., Oxidative stress, inflammation, and cancer: how are they linked? Free Radic. Biol. Med. 49 (2010) 1603-1616 https://doi.org/10.1016/j.freeradbiomed.2010.09.006.

[60] T.Q. Chen, Y.F. Deng, Y.Y. Wang, et al., Butyrolactone I attenuates inflammation in murine NASH by inhibiting the NF-κB signaling pathway, Biochem. Biophys. Res. Commun. 626 (2022) 167-174. https://doi.org/10.1016/j.bbrc.2022.07.050.

[61] Y.E. Chen, S.J. Xu, Y.Y. Lu, et al., Asperuloside suppressing oxidative stress and inflammation in DSS-induced chronic colitis and RAW 264.7 macrophages *via* Nrf2/HO-1 and NF-κB pathways, Chem. Biol. Interact. 344 (2021) 109512. https://doi.org/10.1016/j.cbi.2021.109512.

[62] N. Liu, J. Feng, X. Lu, et al., Isorhamnetin inhibits liver fibrosis by reducing autophagy and inhibiting extracellular matrix formation *via* the TGF-β1/Smad3 and TGF-β1/p38 MAPK pathways, Mediators Inflamm. 2019 (2019) 6175091. https://doi.org/10.1155/2019/6175091.

[63] A.J. Pellicano, K. Spahn, P. Zhou, et al., Collagen characterization in a model of nonalcoholic steatohepatitis with fibrosis; a call for development of targeted therapeutics, Molecules 26 (2021) 3316. https://doi.org/10.3390/molecules26113316.